

# Quantum computation of three-wave interactions with engineered cubic couplings

Yuan Shi,\* Alessandro R. Castelli, Xian Wu, Ilon Joseph, Vasily Geyko, Frank R. Graziani, Stephen B. Libby, Jeffrey B. Parker, Yaniv J. Rosen, Luis A. Martinez, and Jonathan L DuBois  
*Lawrence Livermore National Laboratory, Livermore, California 94551, USA*

(Dated: May 14, 2022)

Quantum simulation hardware usually lacks native cubic couplings, which are essential building blocks in many physics applications. Nevertheless, we demonstrate that effective three-wave vertices can be realized without hardware modification. In particular, for the three-wave Hamiltonian of laser-plasma interactions, we show that its Hilbert space can be decomposed into a direct sum of  $D$ -dimensional subspaces. Within each subspace, physical states are readily mapped to quantum memory, and the Hamiltonian matrix becomes tridiagonal. The resultant unitary evolution is realized using two qubits on state-of-the-art hardware through quantum cloud services, which approximate the three-wave gate as products of  $\sim 20$  standard gates. This trotterization approach allows  $\sim 10$  repetitions of the three-wave gate before results are corrupted by decoherence. As an alternative approach, the unitary evolution is also realized as a single gate using customized control pulses on a transmon qudit. Utilizing the lowest three levels of the qudit, high-fidelity results are obtained for  $\sim 100$  three-wave gate repetitions. Moreover, reliable control pulses may also be synthesized cheaply using interpolation when parameters of the Hamiltonian deviate from those used in numerical optimization. Our results highlight the advantage of using customized gates in physics applications. The generalized multi-wave gates are potentially valuable tools for computing a large class of problems in nonlinear optics, weak turbulence, and lattice gauge theories.

The ability to couple three oscillators is crucial for both the digital and the analog approaches to quantum computing. First, in the digital approach, computation is performed by operating a sequence of standard gates on qubits [1–6]. Gates that operate on three qubits, such as the Toffoli gate, are important for realizing classical logic [7]. Moreover, even for gates that operate on two qubits, a third ancilla qubit is usually necessary for quantum error correction [8–11]. Second, in the analog approach, the quantum hardware is controlled to emulate problems of interest [12–22]. In many physics problems, cubic couplings in the Hamiltonian constitute the lowest-order nonlinearity. Fundamentally, this is because three-field vertices are required to couple fermions with bosons, and mediate boson self interactions in nonabelian gauge theories [23]. On an applied level, three-wave couplings arise for parametric interactions in crystals [24], turbulence cascade in fluids [25], and cross-beam laser energy transfer in plasmas [26]. Therefore, realizing cubic coupling is a major milestone for quantum computing.

However, quantum hardware [27, 28] does not usually provide native cubic couplings. For example, the lowest-order effective Hamiltonian of a superconducting quantum computer may be approximated as [29, 30]

$$H_0 \simeq \sum_j \Omega_j a_j^\dagger a_j + \sum_{j,l} \chi_{jl} a_j^\dagger a_j a_l^\dagger a_l, \quad (1)$$

where we have used the units  $\hbar = 1$  and  $\Omega_j$  is the frequency of the  $j$ -th mode. Notice that the lowest-order nonlinearity is quartic, which is caused by Kerr effects with coupling strength  $\chi_{jl}$ . Given hardware Hamiltonians of this type, qubits are coupled in pairwise manner, and a question that will be answered in this letter is how odd-order couplings may be effectively generated.

As a separate question, are cubic couplings useful resources that can lead to quantum speedup over classical computation? The answer is yes in the context of some important applications. For example, the three-wave equations are solved to (1) optimize the input seed pulse shape when designing nonlinear optical systems in the pump depletion regime [31–33]; (2) determine the turbulence spectrum in the wave-kinetic approach to weak turbulence [34], and (3) compute the energy delivered to the fuel capsule in inertial confinement fusion where lasers exchange energy in plasma [35]. In these applications, the inputs and outputs are simple, while each intermediate step involves  $D \times D$  matrices acting on an initial state  $\psi$ , where  $D$  is the number of wave states. On classical computers, computing  $U_N \dots U_2 U_1 \psi$  involves  $O(ND^2)$  operations, while on quantum processors, assuming that cubic gates are prefabricated, each step only involves the application of  $O(N)$  cubic gates. Therefore, quantum processors may be used as special-purpose accelerators for these calculations, if the same cubic gates are needed repeatedly or new cubic gates can be synthesized cheaply.

In this letter, we demonstrate that effective cubic couplings can be realized without hardware modification and precompiled three-wave gates can be used in subsequent calculations. As an example, consider laser-plasma interactions, which may be a subproblem of some more complex problems. After averaging over fast wave phases, the wave envelopes  $A_j$  satisfy [26]

$$d_t A_1 = g A_2 A_3, \quad (2)$$

$$d_t A_2 = -g^* A_1 A_3^\dagger, \quad (3)$$

$$d_t A_3 = -g^* A_1 A_2^\dagger, \quad (4)$$

where  $d_t = \partial_t + \mathbf{v}_j \cdot \nabla$  is the convective derivative at

the wave group velocity  $\mathbf{v}_j = \partial\omega_j/\partial\mathbf{k}_j$  and  $g$  is the coupling coefficient. The above equations are valid when the positive wave frequencies satisfy the resonance condition  $\omega_1 = \omega_2 + \omega_3$  and the wave vectors satisfy  $\mathbf{k}_1 = \mathbf{k}_2 + \mathbf{k}_3$ .

The above three-wave equations can be derived classically, in which  $A_j$  are complex numbers, as well as quantum mechanically, in which  $A_j$  are operators that satisfy commutation relations  $[A_j, A_l^\dagger] = \delta_{jl}$ . In the later case, consider the temporal problem where spatial derivatives vanish, then the three-wave equations become the Heisenberg equations, where the Hamiltonian is

$$H = igA_1^\dagger A_2 A_3 - ig^* A_1 A_2^\dagger A_3^\dagger. \quad (5)$$

In the more general case where waves have spatial dependencies, the quantum mechanics problem may be promoted to a quantum field theory problem [36]. Due to the limited number of qubits currently available, we will only discuss the temporal problem, which can be mapped to a steady-state 1D problem.

To solve the three-wave problem on quantum processors, a naive approach is to map the wave envelope  $A_j$  to qubit  $a_j$ . However, this mapping has two major limitations. First, the qubit can only be in a superposition of  $|0\rangle$  and  $|1\rangle$  states, while a large amplitude wave, such as that of a laser, involves many photons. Therefore, representing the wave states requires a large number of qubits, and the naive mapping is inefficient. Second, the qubit frequency  $\Omega_j$  is not easily tunable [37] to match  $\omega_j$ . Moreover, it is common that  $\omega_j \gg \omega_k$ , which makes it a stiff problem to emulate  $H$  using  $H_0$ .

Instead of mapping in the energy space, a more useful mapping is in the action space. Due to the special form of  $H$ , the action operators

$$S_2 = n_1 + n_3, \quad (6)$$

$$S_3 = n_1 + n_2, \quad (7)$$

commute with the Hamiltonian, where  $n_j = A_j^\dagger A_j$  is the number operator. We can therefore look for simultaneous eigenstates of  $H$ ,  $S_2$ , and  $S_3$ . The eigenspace has dimension  $D = \min(s_2, s_3) + 1$ , where the integer  $s_j \geq 0$  is the eigenvalue of  $S_j$ . Without loss of generality, suppose  $s_2 \leq s_3$ , which breaks the  $2 \leftrightarrow 3$  symmetry. Then, in the Fock basis  $|n_1, n_2, n_3\rangle$ , any state in the  $D$ -dimensional subspace  $V$  is spanned by

$$|\psi\rangle = \sum_{j=0}^{s_2} c_j |s_2 - j, s_3 - s_2 + j, j\rangle, \quad (8)$$

where the expansion coefficients satisfy the normalization condition  $\sum_j |c_j|^2 = 1$ . It is easy to check that  $S_j|\psi\rangle = s_j|\psi\rangle$ . Moreover, it is important to recognize that  $V$  is a closed subspace under the action of  $H$ , namely,  $H|\psi\rangle \in V$  whenever  $|\psi\rangle \in V$ . Therefore, the total Hilbert space of the three-wave system can be decomposed into a direct sum of invariant subspaces, and

it is sufficient to solve the quantum problem within each subspace. Notice that using  $D$  levels, the above mapping can efficiently represent  $s_3 \gg s_2$  photons.

Moreover, in the invariant subspace, the nonlinear three-wave problem becomes a linear quantum mechanical problem. In the Schrödinger picture,  $i\partial_t|\psi\rangle = H|\psi\rangle$  becomes a system of equations for  $c_j(t)$

$$i\partial_t c_j = igh_{j+\frac{1}{2}} c_{j+1} - ig^* h_{j-\frac{1}{2}} c_{j-1}, \quad (9)$$

where  $h_{j-\frac{1}{2}} = \sqrt{j(s_2 + 1 - j)(s_3 - s_2 + j)}$  with  $h_{-\frac{1}{2}} = h_{D+\frac{1}{2}} = 0$ . Notice that  $H$  is block tridiagonal with zero diagonal elements. Since  $\omega_j$  does not enter, qubits with a fixed set of frequencies  $\Omega_j$  can represent arbitrary three-wave problems.

Once the expansion coefficients are solved for given initial conditions, observables of interest can be evaluated by  $O(D)$  classical operations during post processing. For example, the occupation numbers of the three waves are given by  $\langle n_1 \rangle = \sum_{j=0}^{s_2} (s_2 - j)|c_j|^2$ ,  $\langle n_2 \rangle = \sum_{j=0}^{s_2} (s_3 - s_2 + j)|c_j|^2$ , and  $\langle n_3 \rangle = \sum_{j=0}^{s_2} j|c_j|^2$ . Higher-order cumulants, thereby all possible expectation values of interest, can be obtained similarly, and the three-wave problem is then solved. In other words, by mapping in the action space, the nonlinear three-wave problem is reduced to a linear Hamiltonian simulation problem, whose goal is to determine the final states for given initial states.

To better understand the behavior of the quantum system, let us also analyze it in the Heisenberg picture. In particular, the number operators satisfy

$$\begin{aligned} \partial_t^2 n_1 &= -\partial_t^2 n_2 = -\partial_t^2 n_3 \\ &= 2|g|^2 [s_2 s_3 - (2s_2 + 2s_3 + 1)n_1 + 3n_1^2]. \end{aligned} \quad (10)$$

In comparison, the classical wave action  $I_j = |A_j|^2$ , where  $A_j$  is treated as a complex number, satisfies

$$\begin{aligned} \partial_t^2 I_1 &= -\partial_t^2 I_2 = -\partial_t^2 I_3 \\ &= 2|g|^2 [s_2 s_3 - (2s_2 + 2s_3)I_1 + 3I_1^2]. \end{aligned} \quad (11)$$

The quantum system may be used to approximate the classical system by identifying  $I_j \simeq \langle n_j \rangle$ . The difference is proportional to  $3(\langle n_1^2 \rangle - \langle n_1 \rangle^2) - \langle n_1 \rangle$ . The error term in the parenthesis is small when the state is a well-localized semi-classical state. The second error term is small when stimulated processes dominate spontaneous emission, which occurs when  $s_2$  and  $s_3$  are large. When both errors are small, the system is in the classical regime [38], where the quantum solution approaches the classical solution. In the opposite regime, the behaviors of the two systems are very different. For example, in the thermodynamic limit  $|c_j| = 1/D$ , the quantum system is stationary, whereas the classical system is not. Notice that the classical three-wave problem can always be solved in terms of Jacobi elliptic functions [39, 40].

A nontrivial problem can already be solved using three levels, or equivalently, the  $|00\rangle$ ,  $|01\rangle$ , and  $|10\rangle$  states of

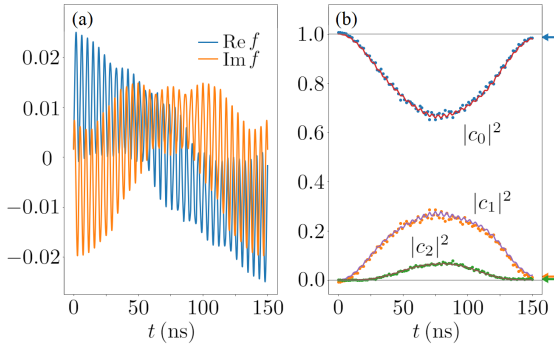


FIG. 1. (a) Optimized control pulse  $f(t)$  for achieving the unitary operator  $U(0.1, \pi/2, 2)$  on the transmon qudit. (b) Experimentally estimated occupations  $|c_n|^2$  (dots) during the control pulse application are well explained by solutions to the master equation (lines). At the end of the pulse, the targeted transition probabilities (arrows) are attained.

two qubits. The allowable dimension is  $D \leq 3$ , and we take  $s_2 = 2$  and  $s_3 = s \geq 2$ . Then, a natural mapping is  $|2, s-2, 0\rangle = (1, 0, 0)^T$ ,  $|1, s-1, 1\rangle = (0, 1, 0)^T$ , and  $|0, s, 2\rangle = (0, 0, 1)^T$ . The normalized Hamiltonian  $h = H/|g|$ , when restricted to the invariant subspace, is

$$h(\theta, s) = \begin{pmatrix} 0 & e^{i\theta}\sqrt{2(s-1)} & 0 \\ e^{-i\theta}\sqrt{2(s-1)} & 0 & e^{i\theta}\sqrt{2s} \\ 0 & e^{-i\theta}\sqrt{2s} & 0 \end{pmatrix}, \quad (12)$$

where  $\exp(i\theta) = ig/|g|$ . This time-independent Hamiltonian can be analytically exponentiated [41] to determine the unitary time-evolution operator  $U(\tau, \theta, s) = \exp[-ih(\theta, s)\tau]$ , where  $\tau = |g|\Delta t$ . In the following, the goal is to realize the three-wave gate  $U(\tau, \theta, s)$  on quantum processors. It is worth emphasizing that the three-level problem is a special example, and a general three-wave gate is associated with a  $D \times D$  unitary matrix. In other words,  $D$  needs not be three, but the Hamiltonian matrix is always tridiagonal, for which there exist efficient numerical algorithms to approximate its exponential [42]. The resultant unitary matrix is an input for quantum compilers.

The standard compilation approach is trotterization, whereby the operator is approximated by products of standard gates. As an example of state-of-the-art quantum cloud services, we implement the three-wave gate on Aspen-4-2Q-A of Rigetti Computing [43, 44]. The probabilistic Quil compiler converts the three-wave gate to a sequence of  $\sim 20$  native gates, including two CZ gates for the three-level problem [45].

As an alternative approach, the unitary operator can also be compiled using control pulse engineering. Instead of preparing control pulses for standard gates and then using them to approximate customized gates, our approach directly prepares control pulses for customized

gates. To demonstrate this approach, the device we use—Quantum Design and Integration Testbed (QuDIT)—is based on a dipole-enhanced Josephson-junction transmon placed inside a 3D superconducting aluminum microwave cavity, whose details are described in [46]. This architecture enhances the coherence time, while minimizing the number of control lines required to access larger computational spaces [47–52]. The control Hamiltonian is [53]

$$H_c(t) \simeq \sum_j (c_j + c_j^\dagger) (f_j e^{-i\Omega_j t} + f_j^* E^{i\Omega_j t}), \quad (13)$$

where the complex-valued  $f_j(t)$  is the slowly-varying envelope of a microwave field whose carrier frequency is  $\Omega_j$  and  $c_j$  is its control operator [54]. Since an arbitrary waveform can be generated by direct digital synthesis, the control is universal [55, 56] and the time dependence of  $f_j(t)$  can be engineered such that

$$\mathcal{T} e^{-i \int_0^T dt [H_0 + H_c(t)]} \simeq e^{-iH\Delta t}, \quad (14)$$

where  $\mathcal{T}$  is the time-ordering operator and  $T$  is the length of the control pulse. The control is not unique and can be designed using numerical optimization [57–61]

As a test problem, we construct a control pulse to achieve  $U(0.1, \pi/2, 2)$ . Based on a thorough characterization of QuDIT that provides parameters of the native Hamiltonian [46], the control pulse is generated using `optimize_pulse_unitary` in QuTIP [62, 63] in the rotating frame. The optimization uses zero as the initial guess, and is constrained by  $|f| < 0.03$ . Two forbidden levels beyond the  $D = 3$  levels are included in the optimization to suppress possible state leakages at the end of the control pulse. The pulse duration ( $T = 150$  ns) is much shorter than the coherence time but long enough to allow the lowest three levels of the transmon, which has an anharmonicity of  $\sim 0.2$  GHz, to be separately addressed. The real and imaginary parts of the optimized pulse are shown in Fig. 1(a), which are obtained after  $\sim 10$  iterations. Further iterations do not significantly improve the fidelity, whose error target is set to be  $10^{-5}$ .

The optimized control pulse is mixed with a carrier at the qudit  $|0\rangle \leftrightarrow |1\rangle$  transition frequency (4.1 GHz), and is compensated for spectral filtering effects of QuDIT. The final waveform is synthesized using an arbitrary waveform generator at 32-GHz sampling rate, and is sent to the qudit inside a dilution refrigerator through a series of attenuators and a band-pass filter. The occupations of the three levels are measured using dispersive readout [47], with a traveling wave parametric amplifier [64, 65] at the base cryogenic temperature and a high-electron-mobility transistor amplifier at 4 K, followed by a room-temperature amplifier. The measured in-phase and quadrature signals are used to classify the states of the qubit, and the classification errors are partially corrected using a confusion matrix [46], which may cause unphysical occupations slightly above 1 or below 0. The

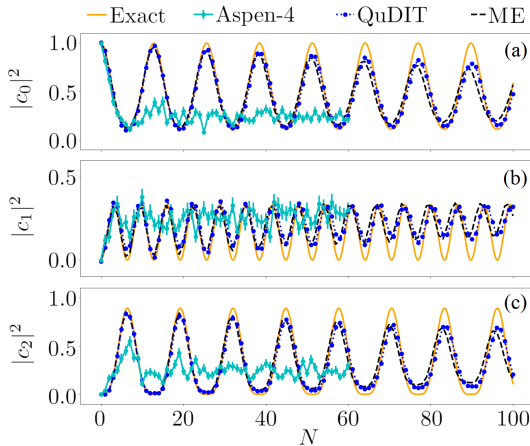


FIG. 2. Occupations of  $|0\rangle$ ,  $|1\rangle$ , and  $|2\rangle$  states after  $N$  repetitions of the three-wave gate  $U(0.2, \pi/2, 2)$ . Using the optimal control approach on QuDIT (blue), the simulation depth is improved by more than ten times compared to using the trotterization approach on Aspen-4 (cyan). Deviations from the exact results (orange) are well explained by solutions of the Lindblad master equation (black).

estimated occupations during the pulse application are shown in Fig. 1(b), when the qudit is initialized in the ground state. The measurement results (dots) are well explained by numerical solutions (lines) of the Lindblad master equation [66–70], when hardware-specific decay and dephasing are taken into account [71]. At the end of the control pulse, the intended unitary operator is realized, and the targeted transition probabilities (arrows) are attained. Using a modified process tomography method [46], we estimate the process matrix of the three-wave gate, which yield an average gate fidelity of 99.3%.

Using either approach, we can now repeatedly apply a prefabricated three-wave gate  $U(0.2, \pi/2, 2)$  for  $N$  times to compute the temporal three-wave problem. With the quantum processors initialized in the ground state, we read out the occupations after  $N$  gate applications, and compare the results with the exact solutions (Fig. 2, orange). Using a customized control pulse ( $T = 80$  ns), the experimental results on QuDIT (blue) follow the exact solutions up to  $N \sim 100$ , and the deviations can be explained by the master equation solutions (black) using our noise model [72]. In comparison, using a sequence of standard gates, the experimental results on Aspen-4 (cyan) track the exact results up to  $N \sim 10$ . However, it is worth emphasizing that the differences are mainly due to the fact that the trotterization approach requires  $\sim 20$  gates while the customized-control approach only requires a single gate for each computational step. In other words, both quantum processors can perform  $\sim 100$  gates with high fidelity, and the better results on QuDIT can mostly be attributed to the control approach instead of the hardware differences.

In addition to reducing the gate depth, the customized-control approach can also alleviate the compilation overhead of parametric gates using interpolation. For example, consider a one-parameter family of three-wave gates  $h(s) = \sqrt{2s}[(1 - \xi)K(2) + (\xi - 1/\sqrt{2})K(\infty)]/(1 - 1/\sqrt{2})$ , where  $\xi(s) = \sqrt{1 - 1/s}$ , and the nonzero elements of the symmetric  $3 \times 3$  matrix  $K$  are  $K_{12}(s) = \xi$  and  $K_{23}(s) = 1$ . Motivated by this form, the interpolated control pulse for  $s \geq 2$  at each time slice is taken to be  $\epsilon_1(s) = [(1 - \xi)\epsilon_0(2) + (\xi - 1/\sqrt{2})\epsilon_0(\infty)]/(1 - 1/\sqrt{2})$ , where  $\epsilon_0(s)$  denotes the optimized pulse, and  $\tau\sqrt{2s} = 0.2$  is held a constant. In other words, we interpolate the control pulse using the same formula for interpolating the Hamiltonian. Although this scheme is not proven to work in general, the interpolated pulses are able to drive high-fidelity results for the three-level problem (Fig. 3). The fidelity is obtained by numerically solving the master equation, and is defined by  $F(\rho, \sigma) = \text{tr}\sqrt{\rho^{1/2}\sigma\rho^{1/2}}$  [7], where  $\rho$  and  $\sigma$  are, respectively, the density matrices attained using optimized and interpolated pulses after one gate application. To optimize control pulses for  $\rho(s)$ ,  $\epsilon_0(2)$  is used as the initial guess.

We would like to thank Rigetti Computing for providing access to their 16Q Aspen-4 processor, where we used lattice Aspen-4-2Q-A. We thank Max D. Porter for verifying numerical results in Figs. 1 and 2. Y. S. would like to thank Eric T. Holland and Hong Qin for helpful discussions. This work was performed under the auspices of US Department of Energy (DOE) by LLNL under Contract DE-AC52-07NA27344. The experimental work was supported by the DOE Office of Fusion Energy Sciences “Quantum Leap for Fusion Energy Sciences” under project FWP-SCW1680, and the theory work was supported by LLNL-LDRD under Project 19-FS-072. The QuDIT was funded under the National Nuclear Security Administration (NNSA) Advanced Simulation and Computing (ASC) “Beyond Moore’s Law” quantum program under NA-ASC-127R-16 and US DOE,

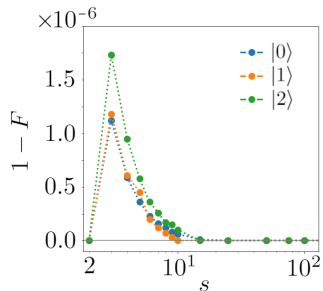


FIG. 3. Interpolated control pulses are able to drive high-fidelity three-wave simulations for a wide range of  $s$  parameters when the qudit is initialized in  $|0\rangle$ ,  $|1\rangle$ , and  $|2\rangle$  states. The interpolation only uses optimized control pulses at  $s = 2$  and  $s = \infty$ , for fixed  $\tau\sqrt{2s} = 0.2$  and  $\theta = \pi/2$ .

Office of Science, Office of Advanced Scientific Computing Research, Quantum Testbed Pathfinder Program under Award 2017-LLNL-SCW1631. Y. S. was supported by the Lawrence Fellowship through LLNL-LDRD under Project 19-ERD-038.

\* shi9@llnl.gov

[1] A. Barenco, C. H. Bennett, R. Cleve, D. P. DiVincenzo, N. Margolus, P. Shor, T. Sleator, J. A. Smolin, and H. Weinfurter, Elementary gates for quantum computation, *Phys. Rev. A* **52**, 3457 (1995).

[2] B. P. Lanyon, C. Hempel, D. Nigg, M. Müller, R. Gerritsma, F. Zähringer, P. Schindler, J. T. Barreiro, M. Rambach, G. Kirchmair, M. Hennrich, P. Zoller, R. Blatt, and C. F. Roos, Universal digital quantum simulation with trapped ions, *Science* **334**, 57 (2011).

[3] M. Mariantoni, H. Wang, T. Yamamoto, M. Neeley, R. C. Bialczak, Y. Chen, M. Lenander, E. Lucero, A. D. O'Connell, D. Sank, M. Weides, J. Wenner, Y. Yin, J. Zhao, A. N. Korotkov, A. N. Cleland, and J. M. Martinis, Implementing the quantum von neumann architecture with superconducting circuits, *Science* **334**, 61 (2011).

[4] U. L. Heras, A. Mezzacapo, L. Lamata, S. Filipp, A. Wallraff, and E. Solano, Digital quantum simulation of spin systems in superconducting circuits, *Phys. Rev. Lett.* **112**, 200501 (2014).

[5] A. Mezzacapo, U. Las Heras, J. Pedernales, L. DiCarlo, E. Solano, and L. Lamata, Digital quantum rabi and dicke models in superconducting circuits, *Sci. Rep.* **4**, 7482 (2014).

[6] Y. Salathé, M. Mondal, M. Oppliger, J. Heinsoo, P. Kurpiers, A. Potočnik, A. Mezzacapo, U. Las Heras, L. Lamata, E. Solano, S. Filipp, and A. Wallraff, Digital quantum simulation of spin models with circuit quantum electrodynamics, *Phys. Rev. X* **5**, 021027 (2015).

[7] M. A. Nielsen and I. Chuang, *Quantum computation and quantum information* (Cambridge University Press, 2010).

[8] N. Ofek, A. Petrenko, R. Heeres, P. Reinhold, Z. Leghtas, B. Vlastakis, Y. Liu, L. Frunzio, S. Girvin, L. Jiang, *et al.*, Extending the lifetime of a quantum bit with error correction in superconducting circuits, *Nature* **536**, 441 (2016).

[9] F. Reiter, A. S. Sørensen, P. Zoller, and C. Muschik, Dissipative quantum error correction and application to quantum sensing with trapped ions, *Nat. Commun.* **8**, 1822 (2017).

[10] S. Rosenblum, P. Reinhold, M. Mirrahimi, L. Jiang, L. Frunzio, and R. J. Schoelkopf, Fault-tolerant detection of a quantum error, *Science* **361**, 266 (2018).

[11] S. Rosenblum, Y. Y. Gao, P. Reinhold, C. Wang, C. J. Axline, L. Frunzio, S. M. Girvin, L. Jiang, M. Mirrahimi, M. H. Devoret, *et al.*, A CNOT gate between multiphoton qubits encoded in two cavities, *Nat. Commun.* **9**, 652 (2018).

[12] R. Gerritsma, G. Kirchmair, F. Zähringer, E. Solano, R. Blatt, and C. F. Roos, Quantum simulation of the Dirac equation, *Nature* **463**, 68 (2010).

[13] Y. Chen, P. Roushan, D. Sank, C. Neill, E. Lucero, M. Mariantoni, R. Barends, B. Chiaro, J. Kelly, A. Megrant, *et al.*, Emulating weak localization using a solid-state quantum circuit, *Nat. Commun.* **5**, 5184 (2014).

[14] P. Roushan, C. Neill, Y. Chen, M. Kolodrubetz, C. Quintana, N. Leung, M. Fang, R. Barends, B. Campbell, Z. Chen, *et al.*, Observation of topological transitions in interacting quantum circuits, *Nature* **515**, 241 (2014).

[15] J. Braumüller, M. Marthaler, A. Schneider, A. Stehli, H. Rotzinger, M. Weides, and A. V. Ustinov, Analog quantum simulation of the Rabi model in the ultra-strong coupling regime, *Nat. Commun.* **8**, 779 (2017).

[16] P. Roushan, C. Neill, J. Tangpanitanon, V. M. Bastidas, A. Megrant, R. Barends, Y. Chen, Z. Chen, B. Chiaro, A. Dunsworth, A. Fowler, B. Foxen, M. Giustina, E. Jeffrey, J. Kelly, E. Lucero, J. Mutus, M. Neeley, C. Quintana, D. Sank, A. Vainsencher, J. Wenner, T. White, H. Neven, D. G. Angelakis, and J. Martinis, Spectroscopic signatures of localization with interacting photons in superconducting qubits, *Science* **358**, 1175 (2017).

[17] P. Roushan, C. Neill, A. Megrant, Y. Chen, R. Babbush, R. Barends, B. Campbell, Z. Chen, B. Chiaro, A. Dunsworth, *et al.*, Chiral ground-state currents of interacting photons in a synthetic magnetic field, *Nat. Phys.* **13**, 146 (2017).

[18] N. Langford, R. Sagastizabal, M. Kounalakis, C. Dickel, A. Bruno, F. Luthi, D. Thoen, A. Endo, and L. DiCarlo, Experimentally simulating the dynamics of quantum light and matter at deep-strong coupling, *Nat. Commun.* **8**, 1715 (2017).

[19] A. Kandala, A. Mezzacapo, K. Temme, M. Takita, M. Brink, J. M. Chow, and J. M. Gambetta, Hardware-efficient variational quantum eigensolver for small molecules and quantum magnets, *Nature* **549**, 242 (2017).

[20] C. Neill, P. Roushan, K. Kechedzhi, S. Boixo, S. V. Isakov, V. Smelyanskiy, A. Megrant, B. Chiaro, A. Dunsworth, K. Arya, R. Barends, B. Burkett, Y. Chen, Z. Chen, A. Fowler, B. Foxen, M. Giustina, R. Graff, E. Jeffrey, T. Huang, J. Kelly, P. Klimov, E. Lucero, J. Mutus, M. Neeley, C. Quintana, D. Sank, A. Vainsencher, J. Wenner, T. C. White, H. Neven, and J. M. Martinis, A blueprint for demonstrating quantum supremacy with superconducting qubits, *Science* **360**, 195 (2018).

[21] R. Harris, Y. Sato, A. J. Berkley, M. Reis, F. Altomare, M. H. Amin, K. Boothby, P. Bunyk, C. Deng, C. Enderud, S. Huang, E. Hoskinson, M. W. Johnson, E. Ladizinsky, N. Ladizinsky, T. Lanting, R. Li, T. Medina, R. Molavi, R. Neufeld, T. Oh, I. Pavlov, I. Perminov, G. Poulin-Lamarre, C. Rich, A. Smirnov, L. Swenson, N. Tsai, M. Volkmann, J. Whittaker, and J. Yao, Phase transitions in a programmable quantum spin glass simulator, *Science* **361**, 162 (2018).

[22] E. T. Holland, K. A. Wendt, K. Kravvaris, X. Wu, W. E. Ormand, J. L. DuBois, S. Quaglioni, and F. Pederiva, Optimal control for the quantum simulation of nuclear dynamics, *Phys. Rev. A* **101**, 062307 (2020).

[23] C.-N. Yang and R. L. Mills, Conservation of isotopic spin and isotopic gauge invariance, *Phys. Rev.* **96**, 191 (1954).

[24] N. Bloembergen, *Nonlinear Optics* (World Scientific, 1996).

[25] V. E. Zakharov, V. L'vov, and G. Falkovich, *Kolmogorov spectra of turbulence* (Springer-Verlag, 1992).

[26] R. Davidson, *Methods in Nonlinear Plasma Theory* (Academic Press, 1972).

[27] H. Häffner, C. F. Roos, and R. Blatt, Quantum computing with trapped ions, *Phys. Rep.* **469**, 155 (2008).

[28] J. Clarke and F. K. Wilhelm, Superconducting quantum bits, *Nature* **453**, 1031 (2008).

[29] J. M. Chow, L. DiCarlo, J. M. Gambetta, F. Motzoi, L. Frunzio, S. M. Girvin, and R. J. Schoelkopf, Optimized driving of superconducting artificial atoms for improved single-qubit gates, *Phys. Rev. A* **82**, 040305 (2010).

[30] S. E. Nigg, H. Paik, B. Vlastakis, G. Kirchmair, S. Shankar, L. Frunzio, M. H. Devoret, R. J. Schoelkopf, and S. M. Girvin, Black-box superconducting circuit quantization, *Phys. Rev. Lett.* **108**, 240502 (2012).

[31] L. M. Frantz and J. S. Nodvik, Theory of pulse propagation in a laser amplifier, *J. Appl. Phys.* **34**, 2346 (1963).

[32] J. Ahn, A. Efimov, R. Averitt, and A. Taylor, Terahertz waveform synthesis via optical rectification of shaped ultrafast laser pulses, *Opt. Express* **11**, 2486 (2003).

[33] G. Brunton, G. Erbert, D. Browning, and E. Tse, The shaping of a national ignition campaign pulsed waveform, *Fusion Eng. Des.* **87**, 1940 (2012).

[34] V. E. Zakharov, V. S. L'vov, and G. Falkovich, *Kolmogorov spectra of turbulence I: Wave turbulence* (Springer Science & Business Media, 2012).

[35] J. F. Myatt, J. Zhang, R. W. Short, A. V. Maximov, W. Seka, D. H. Froula, D. H. Edgell, D. T. Michel, I. V. Igumenshchev, D. E. Hinkel, *et al.*, Multiple-beam laser-plasma interactions in inertial confinement fusion, *Phys. Plasmas* **21**, 055501 (2014).

[36] Y. Shi, H. Qin, and N. J. Fisch, Three-wave scattering in magnetized plasmas: From cold fluid to quantized lagrangian, *Phys. Rev. E* **96**, 023204 (2017).

[37] Y. Chen, C. Neill, P. Roushan, N. Leung, M. Fang, R. Barends, J. Kelly, B. Campbell, Z. Chen, B. Chiaro, A. Dunsworth, E. Jeffrey, A. Megrant, J. Y. Mutus, P. J. J. O'Malley, C. M. Quintana, D. Sank, A. Vainsencher, J. Wenner, T. C. White, M. R. Geller, A. N. Cleland, and J. M. Martinis, Qubit architecture with high coherence and fast tunable coupling, *Phys. Rev. Lett.* **113**, 220502 (2014).

[38] E. T. Jaynes and F. W. Cummings, Comparison of quantum and semiclassical radiation theories with application to the beam maser, *Proc. IEEE* **51**, 89 (1963).

[39] A. Jurkus and P. Robson, Saturation effects in a travelling-wave parametric amplifier, *Proceedings of the IEE-Part B: Electronic and Communication Engineering* **107**, 119 (1960).

[40] J. A. Armstrong, N. Bloembergen, J. Ducuing, and P. S. Pershan, Interactions between light waves in a nonlinear dielectric, *Phys. Rev.* **127**, 1918 (1962).

[41] See Supplemental Material for the unitary matrix of the three-level problem.

[42] F. R. Graziani, The product formula algorithm applied to linear and radiation diffusion, *J. Comp. Phys.* **118**, 9 (1995).

[43] P. J. Karalekas, N. A. Tezak, E. C. Peterson, C. A. Ryan, M. P. da Silva, and R. S. Smith, A quantum-classical cloud platform optimized for variational hybrid algorithms, *Quantum Sci. Technol.* **5**, 024003 (2020).

[44] R. S. Smith, M. J. Curtis, and W. J. Zeng, A practical quantum instruction set architecture (2016), arXiv:1608.03355 [quant-ph].

[45] See Supplemental Material for an example the Quil program.

[46] X. Wu, S. Tomarken, N. A. Petersson, L. Martinez, Y. J. Rosen, and J. L. DuBois, High-fidelity software-defined quantum logic on a superconducting qudit, arXiv:2005.13165 (2020).

[47] A. Blais, R.-S. Huang, A. Wallraff, S. M. Girvin, and R. J. Schoelkopf, Cavity quantum electrodynamics for superconducting electrical circuits: An architecture for quantum computation, *Phys. Rev. A* **69**, 062320 (2004).

[48] A. Wallraff, D. I. Schuster, A. Blais, L. Frunzio, R.-S. Huang, J. Majer, S. Kumar, S. M. Girvin, and R. J. Schoelkopf, Strong coupling of a single photon to a superconducting qubit using circuit quantum electrodynamics, *Nature* **431**, 162 (2004).

[49] J. Koch, T. M. Yu, J. Gambetta, A. A. Houck, D. I. Schuster, J. Majer, A. Blais, M. H. Devoret, S. M. Girvin, and R. J. Schoelkopf, Charge-insensitive qubit design derived from the Cooper pair box, *Phys. Rev. A* **76**, 042319 (2007).

[50] J. A. Schreier, A. A. Houck, J. Koch, D. I. Schuster, B. R. Johnson, J. M. Chow, J. M. Gambetta, J. Majer, L. Frunzio, M. H. Devoret, S. M. Girvin, and R. J. Schoelkopf, Suppressing charge noise decoherence in superconducting charge qubits, *Phys. Rev. B* **77**, 180502 (2008).

[51] H. Paik, D. I. Schuster, L. S. Bishop, G. Kirchmair, G. Catelani, A. P. Sears, B. R. Johnson, M. J. Reagor, L. Frunzio, L. I. Glazman, S. M. Girvin, M. H. Devoret, and R. J. Schoelkopf, Observation of high coherence in josephson junction qubits measured in a three-dimensional circuit QED architecture, *Phys. Rev. Lett.* **107**, 240501 (2011).

[52] C. Rigetti, J. M. Gambetta, S. Poletto, B. L. T. Plourde, J. M. Chow, A. D. Córcoles, J. A. Smolin, S. T. Merkel, J. R. Rozen, G. A. Keefe, M. B. Rothwell, M. B. Ketchen, and M. Steffen, Superconducting qubit in a waveguide cavity with a coherence time approaching 0.1 ms, *Phys. Rev. B* **86**, 100506 (2012).

[53] C. Gerry, P. Knight, and P. L. Knight, *Introductory quantum optics* (Cambridge university press, 2005).

[54] See Supplemental Material for an explicit expression of the control operator.

[55] J. Raftery, A. Vrajitoarea, G. Zhang, Z. Leng, S. Srinivasan, and A. Houck, Direct digital synthesis of microwave waveforms for quantum computing, arXiv:1703.00942 (2017).

[56] R. W. Heeres, P. Reinhold, N. Ofek, L. Frunzio, L. Jiang, M. H. Devoret, and R. J. Schoelkopf, Implementing a universal gate set on a logical qubit encoded in an oscillator, *Nat. Commun.* **8**, 94 (2017).

[57] N. Khaneja, T. Reiss, C. Kehlet, T. Schulte-Herbrüggen, and S. J. Glaser, Optimal control of coupled spin dynamics: design of nmr pulse sequences by gradient ascent algorithms, *J. Magn. Reson.* **172**, 296 (2005).

[58] P. De Fouquieres, S. Schirmer, S. Glaser, and I. Kuprov, Second order gradient ascent pulse engineering, *J. Magn. Reson.* **212**, 412 (2011).

[59] S. Lloyd and S. Montangero, Information theoretical analysis of quantum optimal control, *Phys. Rev. Lett.* **113**, 010502 (2014).

[60] N. Leung, M. Abdelhafez, J. Koch, and D. Schuster, Speedup for quantum optimal control from automatic differentiation based on graphics processing units, *Phys. Rev. A* **95**, 042318 (2017).

[61] N. A. Petersson, F. M. Garcia, A. E. Copeland, Y. L. Rydin, and J. L. DuBois, Discrete adjoints for accurate numerical optimization with application to quantum control, arXiv:2001.01013 (2020).

[62] J. Johansson, P. Nation, and F. Nori, Qutip 2: A python framework for the dynamics of open quantum systems, *Comput. Phys. Commun.* **184**, 1234 (2013).

[63] J. R. Johansson, P. Nation, and F. Nori, Qutip: An open-source python framework for the dynamics of open quantum systems, *Comp. Phys. Commun.* **183**, 1760 (2012).

[64] K. O'Brien, C. Macklin, I. Siddiqi, and X. Zhang, Resonant phase matching of josephson junction traveling wave parametric amplifiers, *Phys. Rev. Lett.* **113**, 157001 (2014).

[65] C. Macklin, K. O'Brien, D. Hover, M. E. Schwartz, V. Bolkhovsky, X. Zhang, W. D. Oliver, and I. Siddiqi, A near-quantum-limited Josephson traveling-wave parametric amplifier, *Science* **350**, 307 (2015).

[66] K. W. Murch, U. Vool, D. Zhou, S. J. Weber, S. M. Girvin, and I. Siddiqi, Cavity-assisted quantum bath engineering, *Phys. Rev. Lett.* **109**, 183602 (2012).

[67] K. Geerlings, Z. Leghtas, I. M. Pop, S. Shankar, L. Frunzio, R. J. Schoelkopf, M. Mirrahimi, and M. H. Devoret, Demonstrating a driven reset protocol for a superconducting qubit, *Phys. Rev. Lett.* **110**, 120501 (2013).

[68] Z. Leghtas, U. Vool, S. Shankar, M. Hatridge, S. M. Girvin, M. H. Devoret, and M. Mirrahimi, Stabilizing a bell state of two superconducting qubits by dissipation engineering, *Phys. Rev. A* **88**, 023849 (2013).

[69] E. T. Holland, B. Vlastakis, R. W. Heeres, M. J. Reagor, U. Vool, Z. Leghtas, L. Frunzio, G. Kirchmair, M. H. Devoret, M. Mirrahimi, and R. J. Schoelkopf, Single-photon-resolved cross-kerr interaction for autonomous stabilization of photon-number states, *Phys. Rev. Lett.* **115**, 180501 (2015).

[70] Z. Leghtas, S. Touzard, I. M. Pop, A. Kou, B. Vlastakis, A. Petrenko, K. M. Sliwa, A. Narla, S. Shankar, M. J. Hatridge, *et al.*, Confining the state of light to a quantum manifold by engineered two-photon loss, *Science* **347**, 853 (2015).

[71] See Supplemental Material for the noise model based on the Lindblad master equation.

[72] See Supplemental Material for the noise model based on the Lindblad master equation.

[73] Rigetti QCS is continuously upgraded and routinely calibrated. For data reported in this paper, the QCS was accessed on January 7th, 2020 at 12:30 PM.

### Unitary evolution of three levels

For the three-level problem, the Hamiltonian matrix [Eq. (12)] can be exponentiated analytically. The Schrödinger time evolution of the three levels is determined by the unitary matrix  $U = \exp(-i\hbar\tau)$ , which is given explicitly by

$$U(\tau, \theta, s) = \begin{pmatrix} \frac{(s-1)\cos\lambda\tau+s}{2s-1} & -ie^{i\theta}\sqrt{\frac{s-1}{2s-1}}\sin\lambda\tau & e^{2i\theta}\sqrt{\frac{s(s-1)}{2s-1}}(\cos\lambda\tau-1) \\ -ie^{-i\theta}\sqrt{\frac{s-1}{2s-1}}\sin\lambda\tau & \cos\lambda\tau & -ie^{i\theta}\sqrt{\frac{s}{2s-1}}\sin\lambda\tau \\ e^{-2i\theta}\sqrt{\frac{s(s-1)}{2s-1}}(\cos\lambda\tau-1) & -ie^{-i\theta}\sqrt{\frac{s}{2s-1}}\sin\lambda\tau & \frac{s\cos\lambda\tau+s-1}{2s-1} \end{pmatrix}, \quad (\text{S.1})$$

where  $\lambda = \sqrt{2(2s-1)}$  is the positive eigenvalue of the Hamiltonian. The above  $3 \times 3$  unitary matrix can be embedded into a two-qubits system by acting it on the  $|00\rangle$ ,  $|01\rangle$ , and  $|10\rangle$  states, while leaving the  $|11\rangle$  state invariant.

The above unitary matrix is an input for both the trotterization and the customized-control approaches. For larger problems, the three-wave Hamiltonian remains tridiagonal, for which there exist efficient numerical algorithms to approximate its exponential [42]. Although it may seem that once the unitary matrix is known, the problem would have already been solved, it is worth noting that the three-wave gate may be a subproblem of some more complex problems. For example, in radiation hydrodynamics, lasers couple via three-wave interactions for given plasma conditions, while the plasma conditions evolve due to laser energy deposition. The self consistent equations may be solved using the splitting algorithm, whose solutions may be written schematically as  $U_N V_N \dots U_1 V_1 U_0 V_0$ , where  $U$ 's are three-wave gates and  $V$ 's are gates that advance the plasma conditions. In problems of this type, knowing  $U$  is an intermediate step towards solving the entire problem, and quantum computing may be used to effectively carry out the matrix multiplications by applying prefabricated gates.

### Realizing three-wave gates on Rigetti QCS

As an example of state-of-the-art quantum cloud services (QCS), Rigetti Computing [43, 44] offers a native gate set consists of single-qubit rotations  $R_x(\theta)$ ,  $R_z(\theta)$ , and two-qubit CZ gates. The Quil compiler uses these gates to approximate other unitary operators using non-deterministic algorithms [44], which efficiently generate approximations for a given error tolerance. In particular, the unitary matrix  $U(\tau, \theta, s)$  can be declared as a user-defined gate via the `DEFGATE` directive in the pyQuil library [44]. After routing to two adjacent qubits on the quantum hardware, the probabilistic compiler typically converts this three-wave gate to a sequence of  $\sim 20$  native gates, including two CZ gates (Fig. S1). When directly repeating the gate in pyQuil, the compiler multiplies  $[U(\tau)]^N = U(N\tau)$  and compiles for  $U(N\tau)$  instead, so the hardware performance is independent of  $N$ . This default simplification, which offloads the burden of computation to classical computers, is suppressed by placing the gate sequence for  $U(\tau)$  within `PRAGMA PRESERVE_BLOCK` and `PRAGMA END_PRESERVE_BLOCK`. In this way,  $[U(\tau)]^N$  is realized on Rigetti's Aspen-4-2Q-A by applying precompiled  $U(\tau)$  for  $N$  times, and the results [73] are shown in Fig. 2

### Noise modeling using Lindblad master equation

Realistic quantum computers are open systems, and coupling to the environment is inevitable during control and readout operations. The state of a quantum processor, which is mixed with the environment, may be characterized by its density matrix. Assuming processes in the environment are stationary and Markovian, then the time evolution of the density matrix may be described by the Lindblad master equation [66–70]

$$\partial_t \rho = i[\rho, H_0 + H_c(t)] + \sum_j (L_j \rho L_j^\dagger - \frac{1}{2} \{L_j^\dagger L_j, \rho\}), \quad (\text{S.2})$$

where we have used the unit  $\hbar = 1$ . The first term is the unitary evolution due to the bare Hamiltonian  $H_0$  of the quantum hardware, as well as the control Hamiltonian  $H_c(t)$  due to the application of the control pulse. In the second term, Lindblad operators  $L_j$  are used to model dissipative processes due to couplings with the environment. The above Lindblad master equation is solved numerically using the built-in function `mesolve` in QuTIP [62, 63].

To determine our hardware-specific Hamiltonians and Lindbladians, the transmon qudit is modeled using the Cooper pair box model whose parameters are measured experimentally [46]. The measurements are made for the lowest three

levels of the qudit and then extrapolated to higher levels. First, the transition frequencies and the effective drive Hamiltonian are measured using Rabi spectroscopy. In the lab frame and in the transmon eigenbasis, keeping the lowest five levels, we approximate

$$H_0 \simeq \begin{pmatrix} 0 & 0 & 0 & 0 & 0 \\ 0 & 25.758 & 0 & 0 & 0 \\ 0 & 0 & 50.099 & 0 & 0 \\ 0 & 0 & 0 & 72.848 & 0 \\ 0 & 0 & 0 & 0 & 93.828 \end{pmatrix}, \quad c \simeq \begin{pmatrix} 0 & 1.000 & 0 & 0 & 0 \\ 0 & 0 & -1.372 & 0 & 0 \\ 0 & 0 & 0 & -1.618 & 0 \\ 0 & 0 & 0 & 0 & 1.781 \\ 0 & 0 & 0 & 0 & 0 \end{pmatrix}, \quad (S.3)$$

where angular frequencies are in units of rad/ns. Second, two Lindbladians are included to model decay and dephasing. The Lindblad operator  $L_1 \sim a$  describes successive decays to lower levels, whose nonzero matrix elements are  $L_1(j, j+1) = 1/\sqrt{T_1(j+1, j)}$ . The Lindblad operator  $L_2 \sim a^\dagger a$  describes dephasing with respect to lower levels, whose nonzero matrix elements are  $L_2(j, j) = 1/\sqrt{T_2^*(j, j-1)}$ . The  $T_1$  decay time is measured by readout delays, and the  $T_2^*$  dephasing time is measured using Ramsey spectroscopy. Keeping the lowest five levels, we approximate

$$L_1 \simeq \begin{pmatrix} 0 & 0.004 & 0 & 0 & 0 \\ 0 & 0 & 0.006 & 0 & 0 \\ 0 & 0 & 0 & 0.007 & 0 \\ 0 & 0 & 0 & 0 & 0.009 \\ 0 & 0 & 0 & 0 & 0 \end{pmatrix}, \quad L_2 \simeq \begin{pmatrix} 0 & 0 & 0 & 0 & 0 \\ 0 & 0.005 & 0 & 0 & 0 \\ 0 & 0 & 0.014 & 0 & 0 \\ 0 & 0 & 0 & 0.045 & 0 \\ 0 & 0 & 0 & 0 & 0.000 \end{pmatrix}. \quad (S.4)$$

Parameters in the Hamiltonians and the Lindbladians may drift over time and change after each cool down. The above parameters were obtained from the QuDIT calibration that was performed immediately before the experimental runs that produced the data reported in the main text.

```

PRAGMA PRESERVE_BLOCK
PRAGMA INITIAL_REWIRING "GREEDY"
1  RZ(pi) 1
2  RX(1.570796326794897) 1
3  RZ(-0.955316618124509) 1
4  RX(1.5707963267948948) 2
5  CZ 1 2
6  RX(pi/2) 1
7  RZ(0.4898979485566355) 1
8  RX(-pi/2) 1
9  RZ(1.4274665982948886) 2
10 RX(pi/2) 2
11 RZ(0.3986464309139781) 2
12 RX(-pi/2) 2
13 CZ 1 2
14 RZ(-2.1862760354652844) 1
15 RX(pi/2) 1
16 RZ(-1.7141260552949014) 2
17 RX(-1.5707963267948963) 2
PRAGMA END_PRESERVE_BLOCK
:
}

DECLARE ro BIT[2]
MEASURE 0 ro[0]
MEASURE 1 ro[1]

```

FIG. S1. An example Quil program that implement a three-wave gate on Rigetti's Aspen-4. In this example,  $U(0.2, \pi/2, 2)$  is approximated by 17 native gates. This gate sequence can be repeated  $N$  times to realize  $U^N$  before the final readout.